Designing Stable Concentric Tube Robots Using Piecewise Straight Tubes

Junhyoung Ha[1] and Pierre E. Dupont[1], *Fellow, IEEE*

***Abstract*—Concentric tube robots experience elastic instability when the potential energy stored in torsional twisting of the tubes is suddenly released. To date, ensuring stability for all possible rotational configurations has involved constraining the precurvatures and / or precurved lengths of the tubes comprising the robot, which results in limitations on robot curvature and workspace. This paper presents a design approach that eliminates the constraints on tube precurvature and length for stable rotation. The idea is to compose designs in which, at every point along the length of a robot, a single tube is precurved and the others are straight. The resulting designs do not experience any precurvature-induced torsional tube twisting and so are stable regardless of precurvature and length. This design concept can be usefully employed at the tip of a robot to provide a large stable range of tip orientation angles. A stability analysis is provided for designs composed of an arbitrary number of tubes and design rules are provided for tube pairs that can produce tip angles varying from zero to a desired maximum value. The method is validated experimentally for a tube pair comprised of three sections.**

***Index Terms*—Concentric Tube Robot, Elastic Stability**

I. INTRODUCTION

MANY clinical applications involve reaching around corners to access surgical targets. Examples include navigating the chambers of the heart during beating-heart interventions [1], [2], transnasal acess of skull base tumors [3], tumor resection in the bladder [4] and single-port laparoscopy [5]. For such applications, continuum robot designs offer the advantages of small diameters and smoothly varying distributed curvatures. While concentric tube robots [6]–[8] offer the potential of being low-cost and simple solutions, they also can exhibit elastic instabilities during which potential energy stored in twisting of the tubes can be suddenly released causing a sudden and unsafe change in tube curvature [6], [7].

For example, a constant precurvature tube pair possesses an instability if the maximum value of the tip orientation angle, θ_{tip}, is designed to be greater than about 79° [6], [10], where θ_{tip}, as shown in Fig. 1, is defined as the angle between a tangent vector at the base of the tubes and a tangent vector at their tips. This limit angle becomes smaller when the tubes have proximal straight transmissions [11], [12]. The instability occurs when the tubes are rotated such that the combined shape approaches a straight configuration. While one can avoid the instability by keeping the tube pair curved, this creates a hole in the center of the workspace.

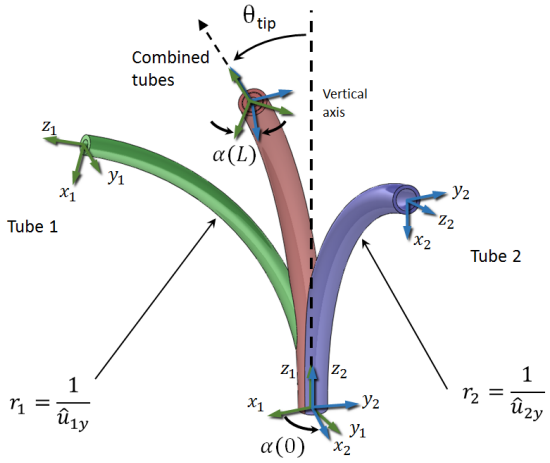

Fig. 1. Tube pair with constant precurvatures. Tip angle, θ_{tip}, is varied by relative rotation of the tubes. Arc length parameter, s, extends from $s = 0$ at the base to $s = L$ at the tip, where L is the length of the tubes. The relative rotation angle between tubes at s, denoted $\alpha_2(s)$, is defined as the rotation angle between the body frames of the tubes at s about their common z-axis. The body frames along each of the tubes are usually chosen as Bishop frames [9].

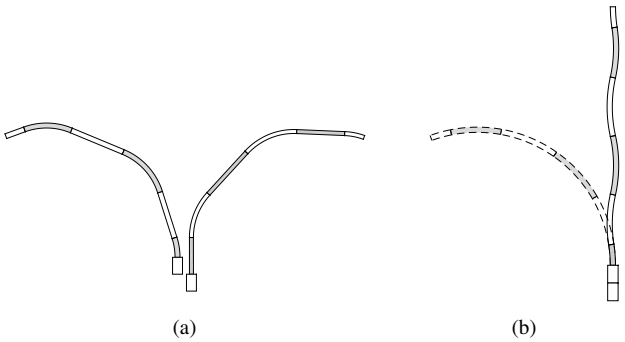

Fig. 2. Piecewise straight tube pair. (a) Individual tubes, (b) Combined tubes. Corresponding tube sections are colored.

Recently, several methods have been proposed to address the instability problem in ways that expand the range of stable angles. These include laser patterning of tubes to change their relative bending and torsional stiffnesses [13], [14] as well as optimizing precurvature as a function of arc length [12], [15]. While laser patterning of tubes has been shown to enhance stability, to date, this has been at the price of substantially

Manuscript received: March, 16, 2016; Revised June, 10, 2016; Accepted August, 12, 2016.

This paper was recommended for publication by Editor Editor name upon evaluation of the Associate Editor and Reviewers' comments. This work was supported by the the NIH under grant R01HL124020.

[1]J. Ha and P. E. Dupont are with the Department of Cardiovascular Surgery, Boston Children's Hospital, Harvard Medical School, Boston, Massachusetts, USA. hjhdog1@gmail.com

Digital Object Identifier (DOI): see top of this page.

reducing bending stiffness. The technique of optimizing tube precurvature does not modify tube properties and successfully increases the range of stable tip angles beyond 79°. One limitation of this method, though, is that tip angle increases as a decreasing function of tube length.

The contribution of this paper is to propose a new design approach that completely eliminates the stability limit on the tip orientation angle. Furthermore, orientation angle increases linearly with tube length. In the proposed approach, depicted in Fig. 2, tube precurvature is selected on a piecewise basis such that only a single tube has a nonzero curvature in each section. This results in global stability. The depicted tube pair is constructed by alternating between zero and maximal precurvature. As shown, careful selection of section lengths enables tip orientation angle to span the interval between its maximum value and zero. At maximum orientation angle, the tube pair is of constant curvature while at zero orientation angle, the shape oscillates in a plane. The price paid for elastic stability is that the combined maximum curvature of the tube pair (dashed configuration in Fig. 2 (b)) is less than the maximum precurvatures of the individual tubes.

The remainder of paper is arranged as follows. Section II provides a stability analysis for both tube pairs and robot designs comprised of an arbitrary number of tubes. The following section provides design rules for tube pairs and compares the proposed approach with constant and optimized precurvature designs. Section III describes experiments on a tube pair designed with the proposed approach. Conclusions appear in the final section.

II. KINEMATICS AND STABILITY OF PIECEWISE STRAIGHT DESIGNS

The mechanics-based model of concentric tube robots incorporating elastic bending and twisting can be described as follows using the notation of [6]. In these equations, the derivative is with respect to arc length and tube curvature is defined with respect to Bishop frames with origins on the the tubes' centerline and with z axes directed tangent to the tubes. The parameters defined below are illustrated in Fig. 1. Precurvature is given as

$$\hat{u}_i(s) = \begin{bmatrix} \hat{u}_{ix}(s) \\ \hat{u}_{iy}(s) \\ 0 \end{bmatrix}.$$

For n tubes, the equations are

$$\begin{aligned} \dot{\alpha}_i &= u_{iz} - u_{1z},\ i = 2, \ldots, n \\ u_{1z} &= (1/k_{1z})(k_{2z}u_{2z} + \ldots + k_{nz}u_{nz}) \\ \dot{u}_{iz} &= (k_{ixy}/k_{iz})\,(u_{ix}\hat{u}_{iy} - u_{iy}\hat{u}_{ix}) \qquad (1) \\ u_i|_{x,y} &= \left(\left(\sum_{j=1}^{n} K_j \right)^{-1} R_z^T(\alpha_i) \left(\sum_{j=1}^{n} R_z(\alpha_j) K_j \hat{u}_j \right) \right) \Bigg|_{x,y} \qquad (2) \end{aligned}$$

with the boundary conditions

$$\begin{aligned} u_{iz}(L_i) &= 0, \qquad (3) \\ \alpha_i(0) &= \theta_{i,\text{base}} - \theta_{1,\text{base}} + u_{iz}(0) l_i, \qquad (4) \end{aligned}$$

where k_{ixy} and k_{iz} are the bending and torsional stiffnesses of tube i, respectively, and $K_i \in \mathbb{R}^{3\times 3}$ is the stiffness tensor of tube i given by

$$K_i = \begin{bmatrix} k_{ixy} & 0 & 0 \\ 0 & k_{ixy} & 0 \\ 0 & 0 & k_{iz} \end{bmatrix}.$$

$\alpha_i(s)$ is relative rotation between tube 1 and tube i, and $u_i(s)$ is 3-dimensional curvature vector of tube i. Here, the rotation of tube i at its base is defined as $\theta_{i,\text{base}}$ and the third term on the right side of (4) is the twist angle of tube i over its straight transmission $s \in [-l_i, 0]$.

Let us first consider the stability of a tube pair of equal length and Poisson's ratio with constant precurvature and stiffnesses, i.e., $L = L_1 = L_2$, $\nu = k_{1xy}/k_{1z} = k_{2xy}/k_{2z}$, $\hat{u}_1(s) = [0\ \hat{u}_{1y}\ 0]^T$ and $\hat{u}_2(s) = [0\ \hat{u}_{2y}\ 0]^T$. In this case, the mechanics-based model incorporating tube bending and twisting reduces to a univariate ODE of the form [6], [10].

$$\ddot{\alpha}_2(s) = (1+\nu)\hat{u}_{1y}(s)\hat{u}_{2y}(s)\sin\alpha_2(s) \qquad (5)$$

with the boundary conditions

$$\begin{aligned} \dot{\alpha}_2(L) &= 0, \qquad (6) \\ \alpha_2(0) &= \alpha_{2,\text{base}} + \frac{k_{1z}}{k_{1z}+k_{2z}}\dot{\alpha}(0) l_2, \qquad (7) \end{aligned}$$

where the base rotation $\alpha_{2,\text{base}}$ is defined as $\alpha_{2,\text{base}} = \theta_{2,\text{base}} - \theta_{1,\text{base}}$.

If the bending stiffnesses and the precurvatures of the tubes satisfy

$$k_{1xy}\hat{u}_{1y} = k_{2xy}\hat{u}_{2y}, \qquad (8)$$

then the configuration of the tube pair varies between the maximally curved configuration and the straight configuration as the bases of the tubes relatively rotate (Fig. 2(a)).

References [6], [10] derive the following stability condition for tube pairs based on the uniqueness of the solution to (5)-(7).

$$L\sqrt{(1+\nu)\hat{u}_{1y}\hat{u}_{2y}} < \pi/2, \qquad (9)$$

This stability condition can be expressed as an upper bound on θ_{tip}. Letting $\bar{u}_y$ denote the maximum combined curvature, $\bar{u}_y$ is given by $\bar{u}_y = \frac{k_{1xy}\hat{u}_{1y} + k_{2xy}\hat{u}_{2y}}{k_{1xy}+k_{2xy}}$ from the bending moment equilibrium between tubes. Substituting this equation and (8) into (9) yields

$$\theta_{\text{tip}} = L\bar{u}_y < \pi \Bigg/ \sqrt{(1+\nu)\left(\frac{k_{1xy}}{k_{2xy}} + \frac{k_{2xy}}{k_{1xy}} + 2\right)} \qquad (10)$$

where θ_{tip} is the angle swept by the combined curvature. Then the right side of (10) is the upper bound of the swept angle. When $k_{1xy} = k_{2xy}$ and $\nu = 0.3$, for example, the upper bound is computed to be 79°.

A. Tube Pair Stability

To solve for any limit imposed on the piecewise straight design, we note that, for any $s \in [0, L]$, these designs satisfy

$$\hat{u}_{1y}(s)\hat{u}_{2y}(s) = 0. \qquad (11)$$

This article has been accepted for publication in a future issue of this journal, but has not been fully edited. Content may change prior to final publication. Citation information: DOI 10.1109/LRA.2016.2606656, IEEE Robotics and Automation Letters

and so (5) reduces to $\ddot{\alpha}_2(s) = 0$. Its solution is now a first-order polynomial of the form

$$\alpha_2(s) = as + b$$

where a and b are constants of integration. Given the boundary conditions (6) and (7), $\alpha_2(s)$ is uniquely determined to be

$$\alpha_2(s) = \alpha_{2,\text{base}}, \quad s \in [0, L].$$

This means that neither tube experiences twist along its length and, consequently, will not experience twist-related instabilities. Thus, the condition (11) is a sufficient condition for solution uniqueness.

B. Stability of Robots Comprised of n Tubes

This result can be generalized to robot designs comprised of n tubes in which only one tube has nonzero precurvature in each section. The precurved tube can be different for different sections of the robot. Assuming that tube q is precurved at s then

$$\hat{u}_{i\neq q} = 0$$

Substituting this equation into (1) yields

$$\dot{u}_{iz} = 0, \quad i \neq q$$

For tube q, note that (2) reduces to

$$u_q(s)|_{x,y} = \frac{k_{qxy}}{k_{I(s)}} R_z^T(\alpha_q) R_z(\alpha_q) \hat{u}_q(s)\big|_{x,y} \tag{12}$$

in which

$$k_{I(s)} = \sum_{i \in I(s)} k_{ixy}$$

and $I(s)$ is the set of indices of tubes existing at s. Substituting this equation into (1) yields that $\dot{u}_{qz} = 0$ and so

$$\dot{u}_{iz} = 0, \quad \forall i \in I(s)$$

Given the boundary condition (3), u_{iz} is given as a constant function by

$$u_{iz}(s) = 0. \tag{13}$$

Thus, none of the tubes experience twist and the kinematic solution is uniquely determined. Concentric tube robots designed in this way are globally stable. We remark that the curved tube can switch to another tube along the length and that there can be arbitrary number of sections separated by these switching points. Note that the precurvature of individual tube sections can be any arbitrary 3D shape.

Another feature of this design is that, theoretically, it requires no torque to quasistatically rotate the tubes with respect to each other. Let E denote the elastic potential energy stored in the tubes, whose explicit formula is given in [7], [16]–[18] by

$$E = \frac{1}{2} \int_0^{L_n} \left\{ \sum_{i \in I(s)} (u_i - \hat{u}_i)^T K_i (u_i - \hat{u}_i) \right\} ds. \tag{14}$$

Substituting (12) and (13) in (14) yields

$$E = \frac{1}{2} \int_0^{L_n} \left\{ \frac{k_{qxy}\left(k_{I(s)} - k_{qxy}\right)}{k_{I(s)}} \right\} u_q^T u_q ds \tag{15}$$

in which q is the index of the tube curved at s, and $I(s)$ and $k_{I(s)}$ are defined as above. Since (15) is a constant function that is invariant to base rotations, $\theta_{i,\text{base}}$, its derivative, $dE/d\theta_{i,\text{base}} = 0$. The torque required to rotate the base of tube i is zero, or equivalently the actuation energy per unit rotation angle is zero. Note that due to friction between the tubes, which is not included in the mechanics-based model above, nonzero actuation torque are required for rotation.

C. Planar Tube Pair Design

For applications such as shown in Fig. 1, it desirable for the robot tip angle, θ_{tip}, to be able to vary continuously over the range $[0, \theta_{\text{tip}}^{\max}]$. Furthermore, when the tip angle is zero, we would like the tip and base tangents to be collinear. Fig. 3 depicts the zero angle configurations that satisfy the latter constraint as the number of sections is varied. The configuration converges to zero curvature along its length as the number of sections increases. Since the curvature of each section is of equal magnitude, the configuration is of constant curvature along its length when the tubes are rotated to achieve $\theta_{\text{tip}}^{\max}$ (dashed configuration in Fig. 2(b)).

To obtain these properties, the lengths of each section, ΔL_k, and precurvatures of each section of tube i, $\hat{u}_{i,k}$, should be selected as follows:

- If the number of section, m, is odd,

$$\begin{aligned} \Delta L_1 &= \Delta L_m, \\ \Delta L_k &= 2\Delta L_1 \text{ for } k = 2, \ldots, m-1, \\ (\hat{u}_{1,k}, \hat{u}_{2,k}) &= (2u_y, 0) \text{ for } k = 1, 3, \ldots, \\ (\hat{u}_{1,k}, \hat{u}_{2,k}) &= (0, 2u_y) \text{ for } k = 2, 4, \ldots. \end{aligned}$$

- If the number of section, m, is even,

$$\begin{aligned} \Delta L_1 &= \Delta L_m, \\ \Delta L_k &= 2\Delta L_1 + a \text{ for } k = 2, m-1, \\ \Delta L_k &= 2\Delta L_1 + 2a \text{ for } k = 3, \ldots, m-2 \\ (\hat{u}_{1,k}, \hat{u}_{2,k}) &= (2u_y, 0) \text{ for } k = 1, 3, \ldots, \\ (\hat{u}_{1,k}, \hat{u}_{2,k}) &= (0, 2u_y) \text{ for } k = 2, 4, \ldots \end{aligned}$$

  where

$$\begin{aligned} a &= \frac{1}{u_y} \cos^{-1}\left(2\cos \Delta L_1 u_y - 1\right) - \Delta L_1, \\ L &= \sum_{k=1}^{m} \Delta L_k \end{aligned} \tag{16}$$

  and $u_y = \theta_{\text{tip}}^{\max}/L$ is the combined curvature and L is the total tube length. Note that L and $\Delta L_{k\neq 1}$ are functions of ΔL_1. When L and $\theta_{\text{tip}}^{\max}$ are given as the design parameters, ΔL_1 is algebraically given for odd m. When m is even, on the other hand, ΔL_1 should be computed as a root of (16).

To maximize θ_{tip}, the nonzero precurvature in each section, $2u_y$, should be selected to be the maximum allowable value. This value can be determined experimentally and is typically limited by, e.g., tube buckling. When combined with a straight tube of equal stiffness, the overall section curvature will be half

This article has been accepted for publication in a future issue of this journal, but has not been fully edited. Content may change prior to final publication. Citation information: DOI 10.1109/LRA.2016.2606656, IEEE Robotics and Automation Letters

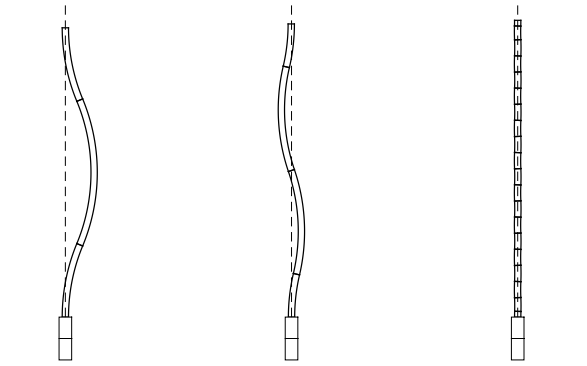

(a) $m = 3$. (b) $m = 4$. (c) $m = 20$.

Fig. 3. Configurations at $\alpha_{w,\text{base}} = \pi$ for variable numbers of sections.

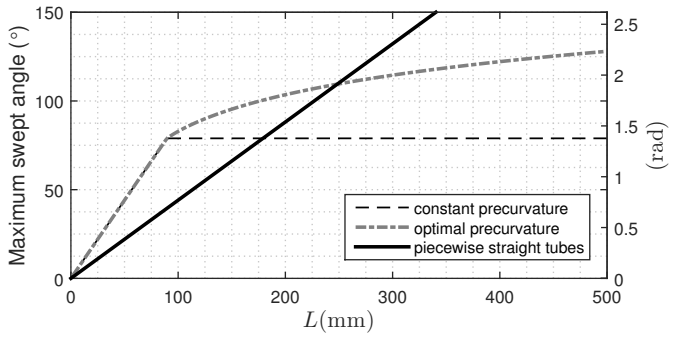

Fig. 4. Maximum tip angle, $\theta_{\text{tip}}^{\max}$, versus tube length, L, for $\nu = 0.3$ and tube precurvature of $1/65\text{mm}^{-1}$.

of the precurvature. This reduction in combined curvature from the precurvature value is the price paid for elastic stability.

The performance of the proposed design is compared to designs of constant and optimized [12], [15] precurvature in Fig. 4 which plots maximum tip angle as a function of tube length. For tip angles up to 79°, the constant and optimized curvature designs are equivalent and their curves possess a slope equal to the allowable precurvature. The slope of the piecewise straight design is half this value and so the maximum angle for a given tube length initially lags the other designs. Since its curve remains linear, however, it outperforms the optimal precurvature design for tip angles above 108° and is the only practical design choice for larger tip angles. Note that this result is independent of the number of sections in the design.

III. EXPERIMENTS

To evaluate the proposed design technique, a three-section tube pair was designed to produce a tip angle range of $\theta_{\text{tip}} \in [0°, 110°]$. The tube and design parameters are given in Table I and the tubes are shown in Fig. 5. The length of section 1 of tube 2 (inner tube) is 17mm longer than the length of section 1 of tube 1 (outer tube) to accommodate the length of the collar used to mount the tube into the drive system. Note that the precurvatures listed are those of the template used in shape setting and that actual precurvatures tend to be smaller due to relaxation that occurs during use.

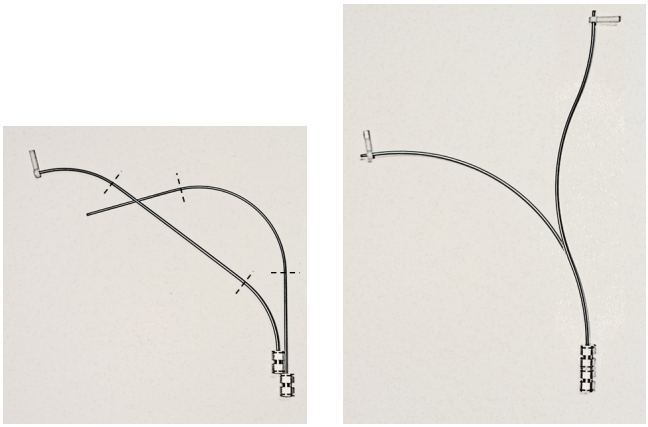

(a) (b)

Fig. 5. Piecewise straight tube pair. (a) Disassembled tubes. (b) Assembled tubes. The dashed lines in (a) represent section boundaries. Two different configurations are superimposed in (b): $\alpha_{2,\text{base}} = 0°$ and 180°.

TABLE I
TUBE PARAMETERS

OD \ ID (mm)	Tube 1	2.540 \ 2.248
	Tube 2	2.083 \ 1.321
Length of tube pair, L (mm)		249.6
Lengths of three sections (mm)	Tube 1	(62.4, 124.8, 62.4)
	Tube 2	(79.4, 124.8, 62.4)
Precurvatures of three sections (mm^{-1})	Tube 1	(1/65, 0, 1/65)
	Tube 2	(0, 1/65, 0)
Angle swept by combined curvature (°)		110
Theoretical Value of Relative Stiffness, k_{xy1}/k_{xy2} and k_{z1}/k_{z2}		1.019
Poisson's Ratio, ν		0.3

The tube pair was then assembled and mounted in the drive system described in [2]. They were rotated through multiple complete revolutions in both directions while logging the tip positions and orientations of both tubes using electromagnetic tracking as shown in Fig. 6. This data was compared with the theoretical behavior predicted by the mechanics-based model to evaluate design stability, torsional twisting of the tubes and accuracy in predicting tip position as described below.

A. Stability

To assess stability, the inner tube was rotated while holding the outer tube fixed. The relative rotation angle between the tubes at their tips is computed from the relative orientation between two EM trackers. Fig. 7 plots a typical data set showings relative rotation angle at the base versus relative rotation angle at the tip as the tube pair undergoes a complete revolution in both directions. Note that the relative rotation angles at the base and at the tip correspond to $\alpha_{2,\text{base}}$ and $\alpha_2(L)$ in the kinematics (5)-(7), respectively. The observed motion was smooth during the experiment and this is reflected by the smooth continuous path plotted in the figure. The actual plot diverges from the unit slope line predicted by the model, however, and displays some hysteresis. Recall that the

This article has been accepted for publication in a future issue of this journal, but has not been fully edited. Content may change prior to final publication. Citation information: DOI 10.1109/LRA.2016.2606656, IEEE Robotics and Automation Letters

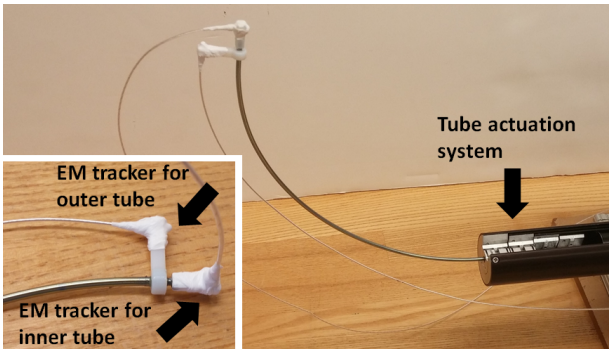

Fig. 6. Experiment setup. Each tube is rotated independently. EM sensors are attached to tube tips using plastic brackets. Inner tube is slightly longer to allow for mounting.

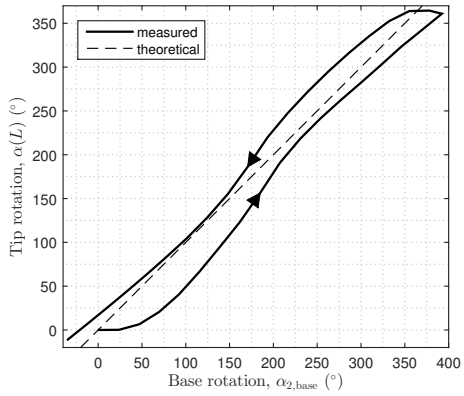

Fig. 7. Relative rotation angle at the base versus the tip for clockwise and counterclockwise rotations. Theoretical unit-slope line is shown dashed.

models of [6], [7] predict tube twisting only as a result of the interaction between tube precurvatures. In reality, friction-inducing contact forces are generated when a curved tube is inserted into a straight tube and it is most likely friction that causes the observed twisting.

To minimize hysteresis in collected data, sets of base rotation angles, $\tilde{\alpha}$, were defined in 10° increments. For each set point, the base rotation angle was commanded to move through a sequence of points that start $\pm 50^\circ$ around the desired set point and converge to the desired point. The sequence is given by

$$\alpha_{2,\text{base},k} = \tilde{\alpha} + 50^\circ(-1)^{k+1}\left(1 - \frac{k}{20}\right) \text{ for } k = 1, \ldots, 20.$$

To avoid any bias due to the direction of the increment, data sets were collected for five revolutions with clockwise increments

$$\tilde{\alpha} = \{360^\circ, 350^\circ, \ldots, 10^\circ, 0^\circ\}$$

and five revolutions with counterclockwise increments

$$\tilde{\alpha} = \{0^\circ, 10^\circ, \ldots, 350^\circ, 360^\circ\}.$$

When each set point was reached, tube tip configuration as reported by the EM trackers was recorded. As shown in Fig. 8, this approach eliminated hysteresis in the ten data sets and also produced highly repeatable results. To verify how much

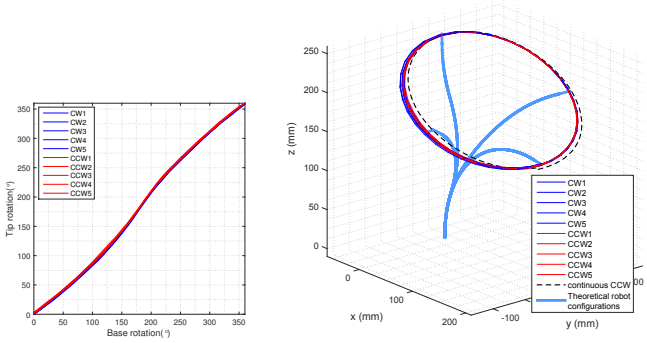

(a) (b)

Fig. 8. Set point data for five clockwise and five counterclockwise rotations. (a) Base versus tip rotation angles. (b) Tip path. Theoretical robot configurations are superimposed in (b).

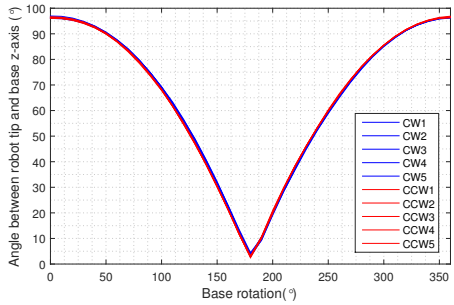

Fig. 9. Tip orientation angle versus base rotation angle. Maximum angle occurs for base rotations of 0° and 360°. Minimum angle corresponds to base rotation of 180°.

the hysteresis affects tip position, we also plot the tip path for continuous tube rotation (continuous CCW) in Fig. 8(b). Notice that the effect of hysteresis on tip position is modest.

This data was examined to determine the range of tip angles that could be achieved. While designed to produce $\theta_{\text{tip}} \in [0^\circ, 110^\circ]$, actual tip angle, plotted in Fig. 9 as a function of base rotation angle, is

$$\theta_{\text{tip}} \in [3.24^\circ, 96.47^\circ].$$

These values differ from the design values due to precurvature relaxation (upper bound) and a slight imbalance between the tubes (lower bound). Nevertheless, this range greatly exceeds what can be stably achieved with tubes of constant precurvature.

To verify how closely this data can be represented by the models of [6], [7], model calibration was performed as described as described below.

B. Calibration

Calibration is formulated as an optimization problem using an objective function defined by the sum of the squared distances between measured and model-predicted tip positions over the 10 data sets:

$$J = \sum_{(\tilde{\alpha},\tilde{p})\in Q} \|\tilde{p} - p_{\text{model}}(\tilde{\alpha})\|^2. \quad (17)$$

This article has been accepted for publication in a future issue of this journal, but has not been fully edited. Content may change prior to final publication. Citation information: DOI 10.1109/LRA.2016.2606656, IEEE Robotics and Automation Letters

TABLE II
CALIBRATED PARAMETERS AND TIP POSITION ERROR OF RIGID-BODY KINEMATICS

Calibrated Parameters	Combined curvature (mm^{-1})	Section 1	1/148.79
		Section 2	1/140.93
		Section 3	1/123.78
Tip position error	Average error (mm)	6.98	
	Maximum error (mm)	15.52	

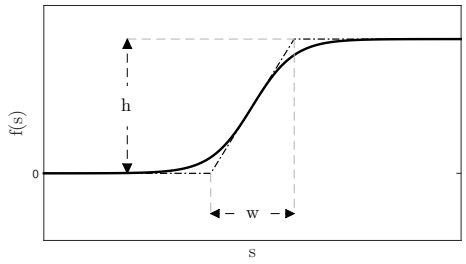

Fig. 10. Sigmoid function for modeling precurvature transitions parameterized by height, h, and width, w.

Here $\tilde{p}$ is the tip position measured by the EM trackers, $p_{\text{model}}(\alpha)$ is the tip position predicted by a model for the base rotation α, and Q is the set of all the measurement pairs $(\tilde{\alpha}, \tilde{p})$.

Calibration was initially performed under the assumption that the tubes possess discontinuities in precurvature at the prescribed positions along their length. In this case, the mechanics-based kinematics predict that the tubes do not twist and the only parameters to be estimated are the combined curvatures for each section. Assuming the combined curvatures are constant along each section, the calibration problem can be formulated as

$$\min_{u_1,u_2,u_3} J$$

where u_1, u_2 and u_3 are the combined curvatures of section $1, 2$ and 3, respectively. Using *fmincon* function in MATLAB as the optimization solver with initial precurvatures selected as half of the nominal values given in Table I, the results of Table II indicate a maximum tip position error of more than 15mm, which is about 6% of the total length of the robot.

The mechanics-based model predicts s-shaped curve, like that of Fig. 8 (a), when tube curvatures overlap. Close inspection of our tubes revealed that, while their shape-setting templates had been machined to produce very sharp changes in curvature, the actual changes in curvature occurred over lengths exceeding 1cm. To investigate this effect, transitions in precurvature were modeled using sigmoid functions of the form

$$f(s) = \frac{h}{1 + e^{-\frac{4s}{w}}},$$

in which w and h are the width and height of the sigmoid as defined in Fig. 10.

The precurvature transitions are modeled with this function centered at the nominal location of the transition. Thus, h represents the nonzero precurvature and w denotes the width of the transition. To reduce the number of calibration parameters and avoid overfitting, the widths of the two transitions on each tube are assumed to be the same, and that the precurvatures of the outer tube at section 1 and section 3 are assumed to be the same as well. This reduces the parameters to four, i.e., the precurvatures of both tubes, $\hat{u}_1$ and $\hat{u}_2$, and the precurvature transition widths of both tubes, w_1 and w_2. The calibration problem is given by

$$\min_{\hat{u}_1,\hat{u}_2,w_1,w_2} J$$

with J given, as before, by (17) and the mechanics-based model is used to compute $p_{\text{model}}(\cdot)$. Using *fmincon* function in MATLAB again with the parameters of Table I and transition widths of 10mm as initial guesses, the calibrated parameters and the average and maximum tip position errors are given in Table III. Both maximum and average error is reduced by slightly more than a factor of two in comparison to the case assuming discontinuous precurvatures.

TABLE III
CALIBRATED PARAMETERS AND TIP POSITION ERROR OF MECHANICS-BASED KINEMATICS

Calibrated Parameters	Precurvatures of curved sections (mm^{-1})	Tube 1	1/74.06
		Tube 2	1/71.48
	Widths of precurvature transition (mm)	Tube 1	19.57
		Tube 2	12.05
Tip position error	Average error (mm)	3.30	
	Maximum error (mm)	6.82	

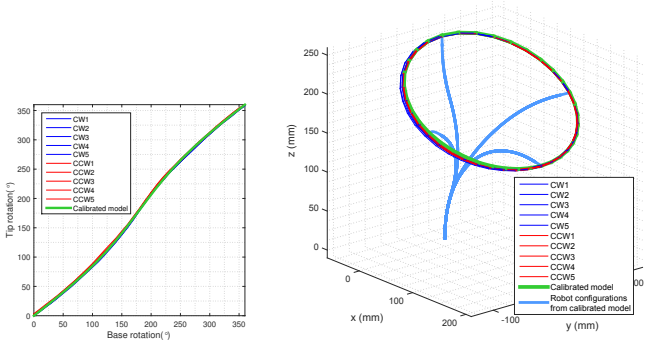

(a) (b)

Fig. 11. Calibrated model using continuous precurvature transitions overlaid on experimental data sets. (a) Base versus tip rotation angles. (b) Tip path.

Fig. 11 overlays the calibrated mechanics-based model with the experimental data sets and shows that the model provides a close fit to the data. While the objective function directly minimizes the error in tip position, it is notable that the base versus tip rotation plots also match the model closely.

IV. CONCLUSION

The proposed design achieves global stability by ensuring that only one tube has nonzero precurvature at any point along the length of the robot. The price of stability is that the combined curvature is always smaller than the individual tube precurvatures. In addition, the "straight" configuration of a tube pair is a sequence of arcs that become straight only as the number of sections approaches infinity.

As shown in our experiments, however, tube pairs with tip angles greater than 90° can easily be constructed. This is an important result since it significantly enlarges the stable workspace of a tube pair.

The experiments also reveal several deficiencies in representing actual robot shape using the current mechanics-based model. In particular, hysteretic tube twisting, potentially due to friction, can be substantial. Furthermore, the assumption that changes in precurvature are discontinuous, which is typically employed with the mechanics-based model, may not be justified in all circumstances.

REFERENCES

[1] N. V. Vasilyev, A. Gosline, A. Veeramani, M. Wu, G. Schmitz, R. Chen, V. Arabagi, P. J. del Nido, and P. E. Dupont, "Tissue removal inside the beating heart using a robotically delivered metal MEMS tool," *Int. J. Robotics Research*, vol. 34, no. 2, pp. 236–247, 2015.

[2] A. H. Gosline, N. V. Vasilyev, E. J. Butler, C. Folk, A. Cohen, R. Chen, N. Lang, P. J. Del Nido, and P. E. Dupont, "Percutaneous intracardiac beating-heart surgery using metal MEMS tissue approximation tools," *The International journal of robotics research*, vol. 31, no. 9, pp. 1081–1093, 2012.

[3] P. J. Swaney, H. B. Gilbert, R. J. Webster III, P. T. Russell III, and K. D. Weaver, "Endonasal Skull Base Tumor Removal Using Concentric Tube Continuum Robots: A Phantom Study," *Journal of Neurological Surgery Part B: Skull Base*, vol. 76, no. 2, pp. 145–149, 2015.

[4] R. E. Goldman, A. Bajo, L. S. MacLachlan, R. Pickens, S. D. Herrell, and N. Simaan, "Design and performance evaluation of a minimally invasive telerobotic platform for transurethral surveillance and intervention," *Biomedical Engineering, IEEE Transactions on*, vol. 60, no. 4, pp. 918–925, 2013.

[5] K. Xu, J. Zhao, and M. Fu, "Development of the sjtu unfoldable robotic system (surs) for single port laparoscopy," *Mechatronics, IEEE/ASME Transactions on*, vol. 20, no. 5, pp. 2133–2145, 2015.

[6] P. E. Dupont, J. Lock, B. Itkowitz, and E. Butler, "Design and control of concentric tube robots," *IEEE Trans. Robotics*, vol. 26, no. 2, pp. 209–225, 2010.

[7] D. C. Rucker, R. J. Webster, G. S. Chirikjian, and N. J. Cowan, "Equilibrium conformations of concentric-tube continuum robots," *The International Journal of Robotics Research*, vol. 29, no. 10, pp. 1263–1280, 2010.

[8] R. Xu and R. Patel, "A fast torsionally compliant kinematic model of concentric-tube robots," in *Engineering in Medicine and Biology Society (EMBC), 2012 Annual International Conference of the IEEE*. IEEE, 2012, pp. 904–907.

[9] R. L. Bishop, "There is more than one way to frame a curve," *Amer. Math. Monthly*, vol. 82, no. 3, pp. 246–251, March 1975.

[10] P. E. Dupont, J. Lock, and E. Butler, "Torsional kinematic model for concentric tube robots," in *Robotics and Automation, 2009. ICRA'09. IEEE International Conference on*. IEEE, 2009, pp. 3851–3858.

[11] R. Xu, S. F. Atashzar, and R. V. Patel, "Kinematic instability in concentric-tube robots: Modeling and analysis," in *Biomedical Robotics and Biomechatronics (2014 5th IEEE RAS & EMBS International Conference on*. IEEE, 2014, pp. 163–168.

[12] J. Ha, F. C. Park, and P. E. Dupont, "Optimizing tube precurvature to enhance elastic stability of concentric tube robots," *Robotics, IEEE Transactions on*, 2016 (in press).

[13] H. Azimian, P. Francis, T. Looi, and J. Drake, "Structurally-redesigned concentric-tube manipulators with improved stability," in *Intelligent Robots and Systems (IROS 2014), 2014 IEEE/RSJ International Conference on*. IEEE, 2014, pp. 2030–2035.

[14] D.-Y. Lee, J. Kim, J.-S. Kim, C. Baek, G. Noh, D.-N. Kim, K. Kim, S. Kang, and K.-J. Cho, "Anisotropic patterning to reduce instability of concentric-tube robots," *Robotics, IEEE Transactions on*, vol. 31, no. 6, pp. 1311–1323, 2015.

[15] J. Ha, F. C. Park, and P. E. Dupont, "Achieving elastic stability of concentric tube robots through optimization of tube precurvature," in *Intelligent Robots and Systems (IROS 2014), 2014 IEEE/RSJ International Conference on*. IEEE, 2014, pp. 864–870.

[16] J. Lock, G. Laing, M. Mahvash, and P. E. Dupont, "Quasistatic modeling of concentric tube robots with external loads," *IEEE/RSJ Int. Conf. Intelligent Robots and Systems*, pp. 2325–2332, 2010.

[17] D. C. Rucker, B. A. Jones, and R. J. Webster III, "A geometrically exact model for externally-loaded concentric-tube continuum robots," *IEEE Trans. Robotics*, vol. 26, no. 5, pp. 769–780, 2010.

[18] J. Ha, F. C. Park, and P. E. Dupont, "Elastic stability of concentric tube robots subject to external loads," *Biomedical Engineering, IEEE Transactions on*, 2015.